JOURNAL OF SPACECRAFT AND ROCKETS
Vol. 29, No. 3, May-June 1992

Basic Experiment on a Supersonic Vortex Flow Around a Missile Body

Didier Pagan,* Pascal Molton,† and Jean Délery‡
Office National d'Etudes et de Recherches Aérospatiales, 92300 Châtillon, France

An experimental study of the flowfield around a three-caliber tangent ogive-cylinder body in a supersonic flow has been made to provide a consistent description of the flow. This experiment includes oil flow visualizations, primary separation line determination, surface pressure measurements, and five-hole pressure probe surveys for a Mach number of 2 and an angle of attack varying from 0 to 20 deg. Results are obtained for a laminar boundary layer over the whole body and for triggered transition. At low-to-moderate incidence (up to 10 deg), the flow structure includes a primary and a secondary vortex. At higher incidences, a complex substructure is also present. The greatest differences occur between laminar boundary layer and turbulent flow cases: at $\alpha = 5$ deg no separation exists in the turbulent case; at $\alpha = 10$ deg, the primary separation appears farther in the leeward direction with smoother velocity gradients in the vortex structure for the turbulent case.

I. Introduction

BOUNDARY-LAYER separation occurring on a missile body at moderate or high angle of attack leads to the formation of well-organized vortical structures, especially at supersonic flight Mach numbers. This phenomenon, in which separation takes place on a smooth surface, is commonly computed by the two following numerical approaches.

For complex industrial applications, in which the computing time is an important parameter, codes solving the Euler equations can constitute very useful tools. However, in any perfect fluid model a special treatment is necessary to introduce the viscous separation process when it occurs on a smooth surface. A generally adopted solution consists in prescribing the velocity direction along the separation line. The location of the separation line itself is obtained either from experimental data bases[1] or deduced from a three-dimensional boundary-layer calculation. In this second circumstance, a coupling technique can be used to take into account the interaction between the boundary layer and the outer inviscid flow.[2,3]

A more satisfactory approach is to solve the time-averaged Navier-Stokes equations, this approach being of course much more expensive in terms of computer time. Navier-Stokes codes applied to the prediction of the flow past missiles have already given interesting results,[4,5] but further studies are needed to obtain precise, effective, and predictable numerical tools. Furthermore, the problem of turbulence modeling for this kind of flow is still largely open.

Hence, improvement and validation of the aforementioned methods require as complete as possible experimental descriptions of the flow around missile-type bodies at incidence. The data base to be constituted should include detailed surface pressure distributions, fine surface flow visualizations to determine the separation lines, and also accurate external flowfield measurements to define the vortex pattern.

Even though a certain number of experimental results are available for this type of flow,[6-10] none of the published data provide the complete set of information for a supersonic flow. This paper gives the main results and conclusions of a study performed with the aim of filling this gap. Furthermore, the effect of the nature of the boundary layer (laminar or turbulent) on the primary separation line location and on the external flowfield structure has also been studied.

II. Experimental Setup and Test Conditions

These experiments have been executed in a continuous return supersonic wind tunnel powered by a 12-stage, 1400-kW axial compressor. The circuit is supplied with desiccated air. The Mach number of the test section can be adjusted in the range 1.6-3.2 by changing the two-dimensional nozzle blocks. The area of the test section is 300×300 mm^2. At the nozzle entrance, the freestream turbulence is inferior to 1%.

The model used for the present study is a nine-caliber ogive-cylinder body equipped with a three-caliber circular ogive. The characteristics of the incoming freestream have been fixed as follows:

Mach number $M_0 = 2$
Stagnation pressure $p_{st0} = 0.05$ MPa
Stagnation temperature $T_{st0} = 330$ K

The model has a length $L = 270$ mm and a diameter $D = 30$ mm. The Reynolds number calculated with D is $Re_D = 0.16 \times 10^6$.

As shown in Fig. 1, the model was sting mounted and its incidence α could be varied from 0 deg to a maximum of 20 deg, dictated by wall interference effects. Two models of identical shape have been manufactured. The first model, equipped with 17 pressure taps equally distributed along a meridian line, has been used for surface pressure measurements. As the flowfield was symmetric for the tested conditions, it was possible to determine the surface pressure distribution by rotating the model around its roll axis. This technique allows a large number of measurements to be made with few pressure taps.

The second model was used to make surface flow visualizations with an oil flow technique. It was equipped with only three pressure taps to check that the flow was not affected when the model was changed.

Experiments have been performed for the two following conditions: natural transition and transition triggered by means of a 5-mm-wide carborundum strip located 30 mm downstream of the body apex. For natural transition, acenaphtene coating visualization enabled us to verify that the boundary layer remained laminar over the entire body at $\alpha = 0$ deg. It has also been verified by using the acenaphtene tech-

Presented as Paper 91-0287 at the AIAA 29th Aerospace Sciences Meeting, Reno, NV, Jan. 7-10, 1991; received April 15, 1991; revision received Jan. 2, 1992; accepted for publication Jan. 31, 1992.

*Research Scientist, Aerodynamics Department; currently Head, Theoretical Aerodynamics Branch, Aérospatiale Missiles Company.
†Principal Technician, Aerodynamics Department.
‡Research Division Head, Aerodynamics Department. Member AIAA.

nique that transition occurred at the location of the carborundum strip for all incidences. Oil flow visualizations allowed the skin friction line patterns to be determined for $\alpha = 5$, 10, 15, and 20 deg.

The external flow has been investigated by means of a miniature five-hole pressure probe having a diameter of 1.5 mm. By proper calibration, this probe allows the determination of the local static and stagnation pressures that give the local Mach number. Then the velocity vector modulus is deduced under the assumption of a constant stagnation temperature, which is a good approximation for moderate incoming freestream Mach number.[11] The calibration also allows the definition of the velocity vector direction with respect to the probe axis. The various quantities given by the five-hole pressure probe are determined with an accuracy of a few percent (2–3%) in regions where gradients are moderate. This accuracy can be estimated in the range 5–10% in the core of the more intense vortices due to the existence of very high gradients. The surveys have been carried out in planes perpendicular to the body axis, along radial lines. Points were clustered near the body surface. At each incidence, 4 to 7 planes have been surveyed, each one including 400 to 900 measurement points. Due to flow symmetry and accessibility, only the upper left quadrant has been probed.

III. Skin Friction Line Pattern Visualizations

Surface flow visualizations have been made for $\alpha = 5$, 10, 15, and 20 deg for both the laminar and the turbulent boundary layer. Top and side photographs of the surface patterns are presented in Fig. 2 for the case of a laminar boundary layer. These visualizations allow the determination of the conjectural skin-friction line patterns represented in the same figure.

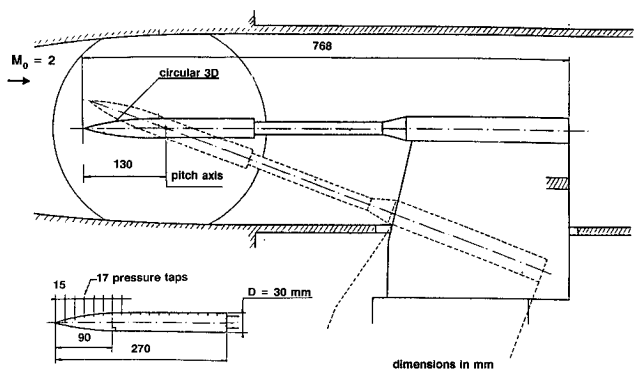

Fig. 1 Model definition and setup main dimensions.

Skin-friction line patterns are topologically equivalent for $\alpha = 5$ and 10 deg. They can be described as follows. All of the skin-friction lines start at the model apex. An attachment line A_1 is present in the windward symmetry plane. Primary separation occurs along line S_1. An attachment line A_2 is visible in the leeward symmetry plane. A second separation occurs along the secondary separation line S_2. Between S_2 and S_1 a third attachment line A_3 must exist. This line is barely visible on the visualizations, since the friction forces in this low-velocity region are not large enough to drive the oil. The separation line S_1, like all of the other skin-friction lines, originates at the apex. However, it can be observed that the skin-friction lines do not converge towards S_1 before $X/D = 4$ ($\alpha = 5$ deg) or $X/D = 3$ ($\alpha = 10$ deg). This region, where skin-friction lines merge together, is the location of the macroscopic separation of the flow. Before this region, a separation line exists but does not induce boundary-layer separation. Similar interpretations are given by other investigators.[12-14]

The transverse flow organization represented in Fig. 3a is deduced from the skin-friction line patterns of Figs. 2a and 2b. It includes one saddle point in the outer flow, five half saddle points on the body (for one-half off the model) and two foci. A perspective view of this situation is given in Fig. 3c. Thus, the separation lines S_1 and S_2 are the traces on the surface of two separation surfaces that roll up to constitute two vortices. This conjectural pattern of the external flowfield is consistent with five-hole probe measurements presented in Sec. V.

For higher angles of attack ($\alpha = 15$ and 20 deg, Figs. 2c and 2d), the primary separation line S_1 is clearly visible starting from the apex. The singular lines A_1, A_2, S_2, and A_3 are also present. However, between S_2 and A_3, two other separation lines S_3 and S_4 are visible. Different external flow topologies are compatible with this surface pattern. One of them, showing four foci and two saddle points imbedded in the transverse flowfield, is represented in Fig. 3b. The presence of the second saddle point has been confirmed by the flowfield measurements presented in Sec. V.

Visualizations made with the carborundum strip present have revealed similar patterns for $\alpha = 15$ and 20 deg. At 5 deg

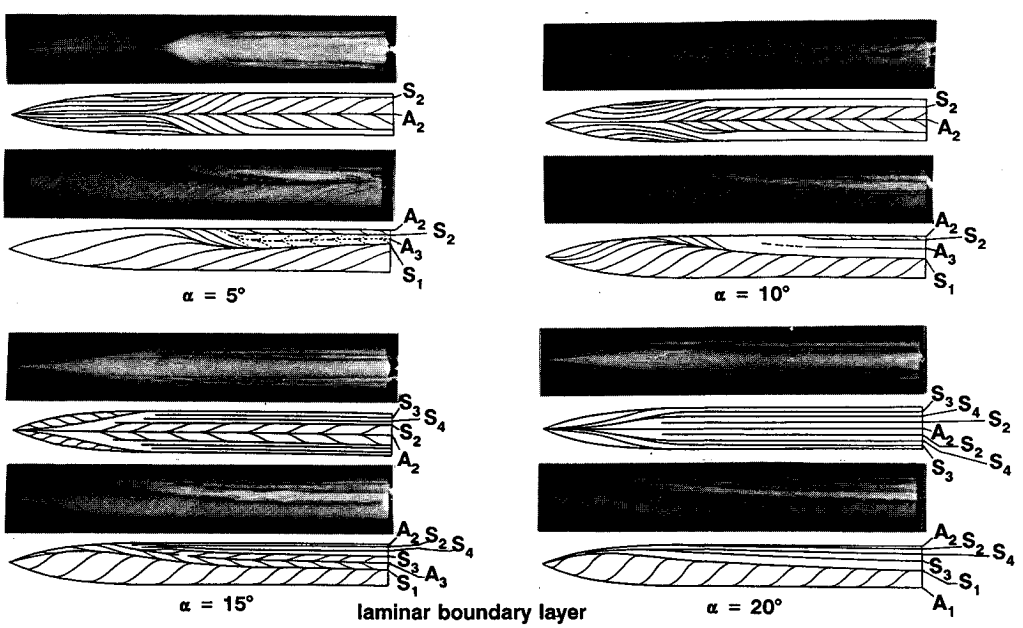

Fig. 2 Skin friction pattern: oil flow visualizations and interpretations.

angle of attack the flow is fully attached and there is no separation, since turbulence tends to stabilize the boundary layer. At $\alpha = 10$ deg, the oil flow visualization is similar to the one observed at $\alpha = 5$ deg for a laminar boundary layer.[15,16]

The location of the primary separation line S_1 has been carefully determined on the model itself. The results thus obtained are plotted in Fig. 4 for the laminar and turbulent boundary-layer cases. We observe that the origin of S_1 comes up to the body apex when incidence is increased and reaches it for $\alpha = 20$ deg. In the laminar case, the separation lines determined at $\alpha = 10$, 15, and 20 deg are very close to each other. In the turbulent case, separation line locations obtained at $\alpha = 10$, 15, and 20 deg are similar to those determined at $\alpha = 5$, 10, and 15 deg, respectively, in the laminar case.

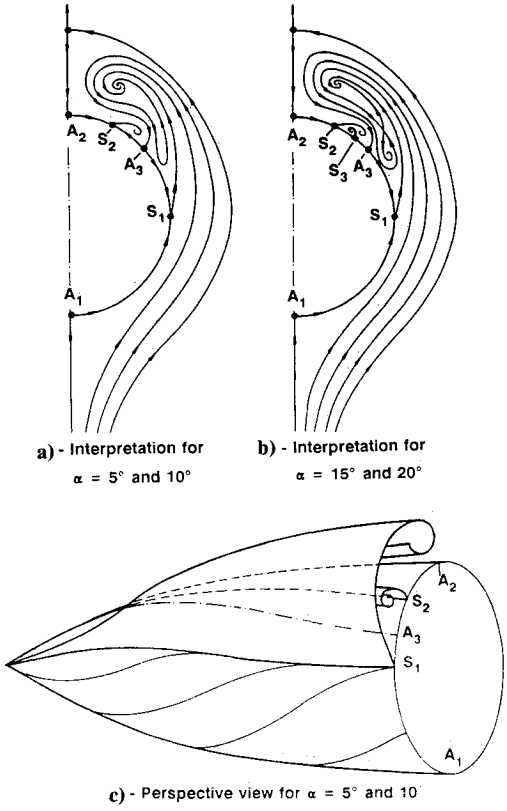

Fig. 3 Conjectural pattern of the external flowfield.

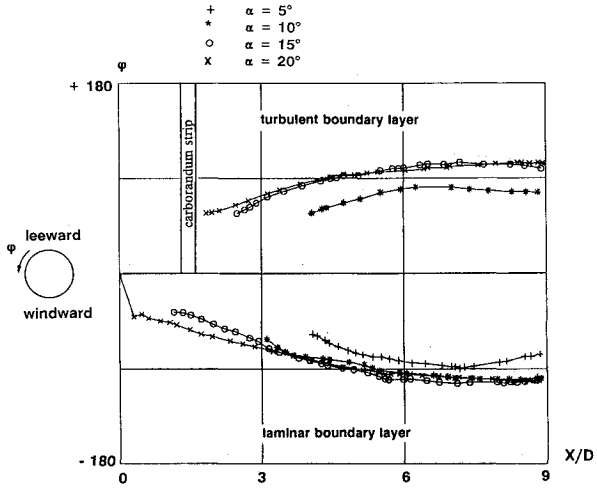

Fig. 4 Primary separation line location.

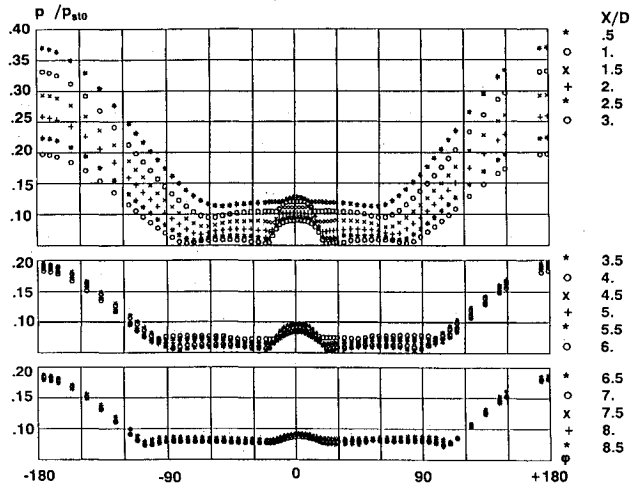

Fig. 5 Surface pressure distribution at $\alpha = 20$ deg for a laminar boundary layer.

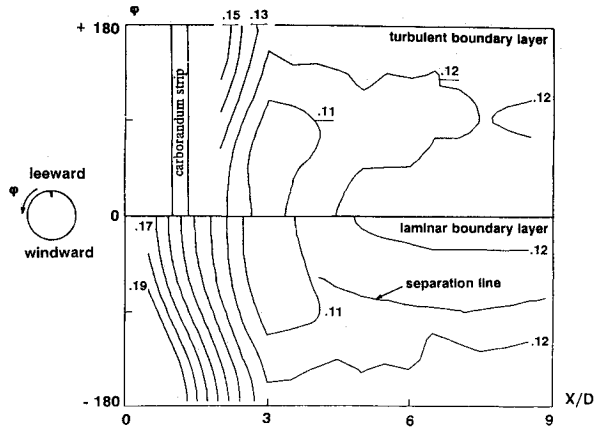

Fig. 6 Iso p/p_{st0} at 5 deg angle of attack.

IV. Surface Pressure Measurements

As stated in Sec. I, the surface pressure distribution has been obtained by rotating the model around its roll axis. The symmetry of the flow is verified a posteriori. For example, Fig. 5 shows plots of surface pressure distributions for $\alpha = 20$ deg angle of attack and a laminar boundary layer. Density and symmetry of measurements are well illustrated. Lines of constant value of the reduced static pressure p/p_{st0} in the $(X/D, \varphi)$ plane have been plotted in Figs. 6–9. The primary separation line location is also represented in these figures. Each figure compares results obtained at the same incidence for a laminar and turbulent boundary layer.

At $\alpha = 5$ deg (see Fig. 6), it appears that the pressure contour plots are very similar, though separation occurs only in the laminar case. In fact, separation does not produce an intense vortex as it does at higher incidences, and therefore it does not affect the pressure distribution.

Visible differences are found at $\alpha = 10$ deg (see Fig. 7). In the laminar case, separation on the leeward side is followed by a plateau of almost constant pressure ($p/p_{st0} = 0.1$) preceding a steep pressure rise. This plateau of relatively low pressure is induced by the presence of a vortex. In the turbulent case, the contour lines are almost regularly spaced between the lowest pressure value of 0.09 and the value in the leeward symmetry plane. The vortex induced by separation being weaker than in the laminar case, its influence on the surface pressure distribution is less pronounced.

Results obtained at $\alpha = 15$ and 20 deg are almost identical (see Figs. 8 and 9). From $X/D = 3$ to the body extremity, the

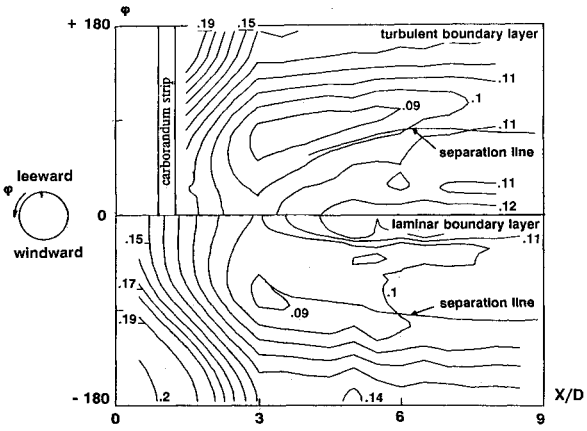

Fig. 7 Iso p/p_{st0} at 10 deg angle of attack.

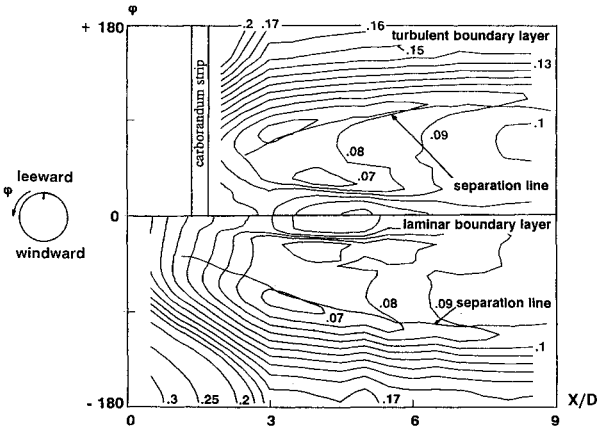

Fig. 8 Iso p/p_{st0} at 15 deg angle of attack.

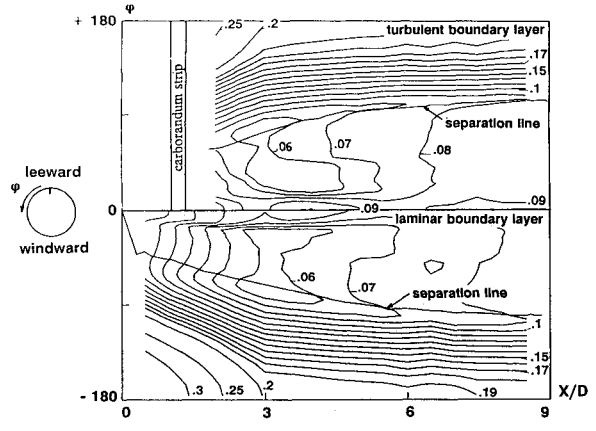

Fig. 9 Iso p/p_{st0} at 20 deg angle of attack.

vortices induce a plateau of low pressure followed by a rapid recompression near $\varphi = 0$ deg. This effect is progressively smoothed out when going downstream, as the vortex moves away from the body.

V. External Flowfield Measurements

Measurements made with the five-hole pressure probe have been performed in planes normal to the body axis for $\alpha = 5$, 10, 15, and 20 deg; both the laminar and the turbulent boundary-layer cases were included. Examples of the results obtained in the plane located at $X/D = 5$ at $\alpha = 20$ deg and for the laminar case are given in Figs. 10 and 11.

Figure 10a shows the plot of the velocity projection in a plane perpendicular to the body axis. The trajectography of this experimental velocity field has been determined by a numerical technique and plotted on the same figure. These plots reveal an organization of the transverse flow that is consistent with the interpretation given in Fig. 3b and reproduced in Fig. 10b. In particular, the foci F_1^*, F_2^*, and F_3^* and the saddle points S_1^* and S_2^* are clearly visible in Fig. 10a. As shown in Fig. 10c, another topological interpretation of the flow structure in a transverse plane can be conceived. In this alternate interpretation, there are only three foci in the outer flow, saddle point S_2^* having disappeared. This structure is consistent with the surface flow pattern and most of the features of the measured velocity fields. However, these measurements show in a rather unambiguous way existence of S_2^* (see Fig. 10a). Thus interpretation shown in Fig. 10b seems to be the most probable, even though it corresponds to a rather complex pattern. This point should be elucidated by further experiments, including vapor screen or laser sheet visualizations. Contour lines of the stagnation pressure and Mach number are presented in Figs. 11a

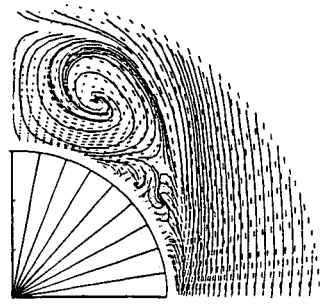

a) Transverse velocity field and associated stream lines

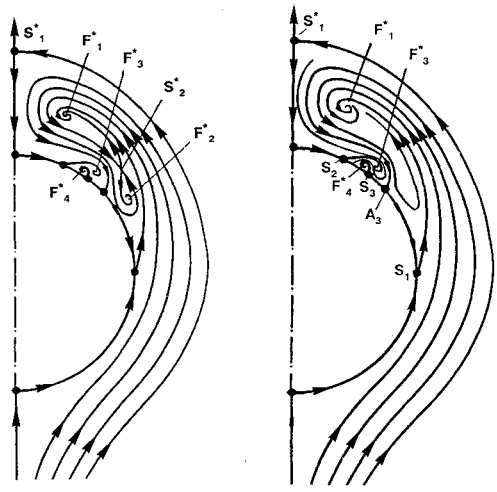

b) Interpretation **c) Alternate interpretation**

Fig. 10 Transverse flowfield properties at $\alpha = 20$ deg, $X/D = 5$ plane, laminar boundar layer.

a) Stagnation pressure (p_{st}/p_{st0}) **b) Mach number**

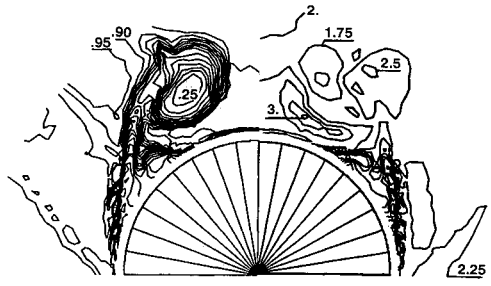

Fig. 11 Transverse flowfield properties at $\alpha = 20$ deg, $X/D = 5$ plane, laminar boundar layer (continued).

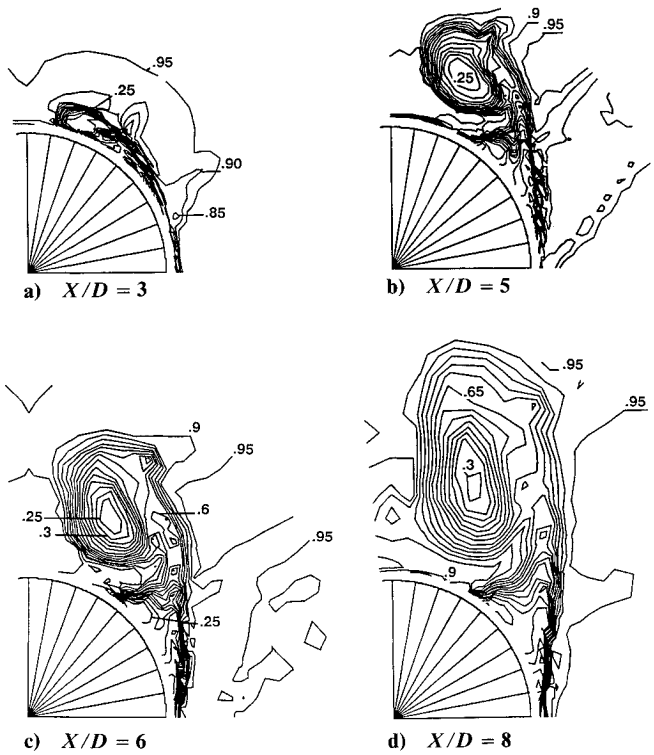

Fig. 12 Evolution of stagnation pressure (p_{st}/p_{st0}) with X/D at $\alpha = 20$ deg, laminar boundary layer.

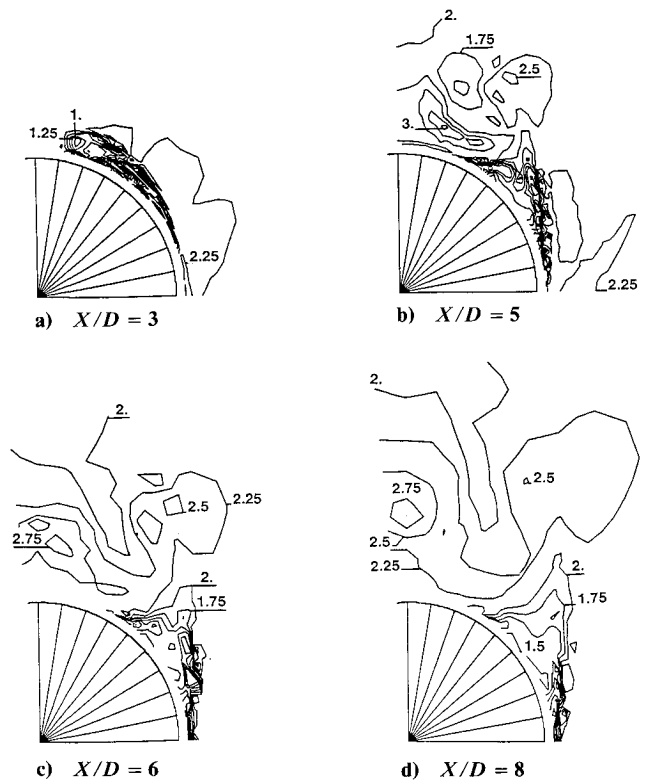

Fig. 13 Evolution of Mach number with X/D at $\alpha = 20$ deg, laminar boundary layer.

and 11b. The boundary layer separates in the vicinity of the horizontal symmetry plane of the figure. The separated sheet springs up and rolls up to constitute the primary vortex. The sheet is a region of high viscous dissipation, as is the primary vortex core (p_{st}/p_{st0} as low as 0.2). High values of Mach number (near 3) are measured under the primary vortex. Secondary separation occurs approximately at 30 deg from the vertical symmetry plane. It produces a secondary vortex characterized by low values of the axial velocity, Mach number, and stagnation pressure. Lastly, the saddle point introduced in Fig. 3b appears in the pseudostreamline plot of Fig. 10, just above a third vortex.

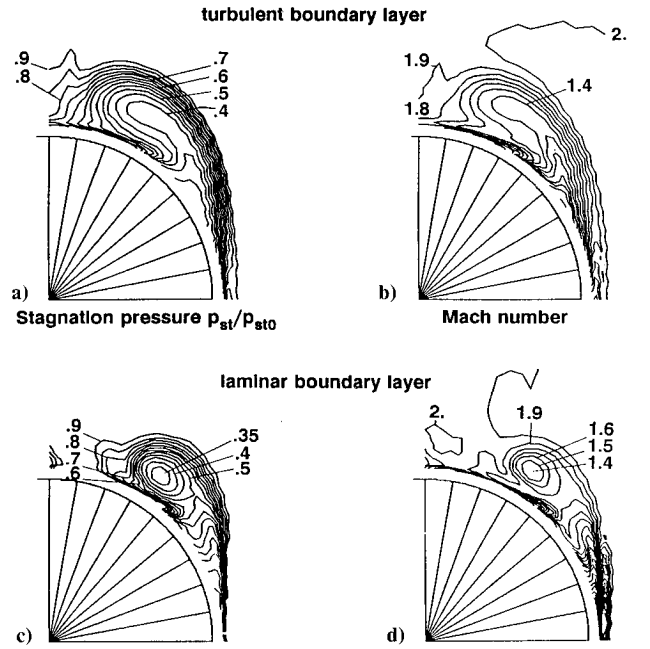

Fig. 14 Comparison between laminar and turbulent boundary layer; $\alpha = 10$ deg, $X/D = 7$.

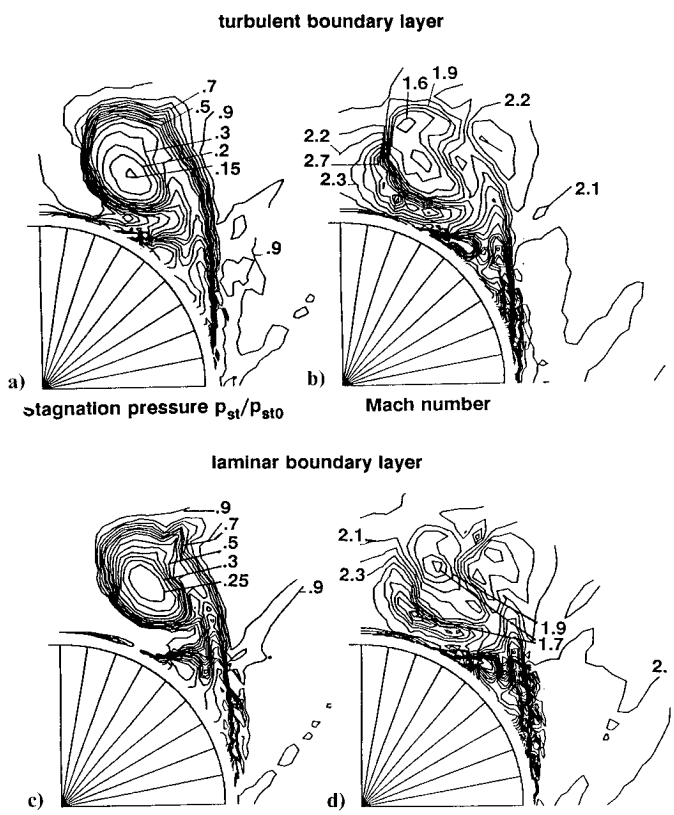

Fig. 15 Comparison between laminar and turbulent boundary layer; $\alpha = 20$ deg, $X/D = 5$.

Figures 12 and 13 show the evolution of the stagnation pressure and Mach number spatial distributions with X/D at 20 deg angle of attack for the laminar case. The stagnation pressure distribution (see Fig. 12) reveals the external envelope of the vortical structures. The primary vortex emerges from the boundary layer at $X/D = 3$. Then the whole vortical structure appears well organized. Further downstream, the primary vortex increases in size and moves away from the body. As shown in Fig. 13, the Mach number evolution is more complex. In this figure, values of Mach number higher than 2.5 exist in some regions of the flow. We can observe that two trends are common from $X/D = 5$ to $X/D = 8$. First, a region of low Mach number exists between the primary and secondary separation lines; second, high Mach number values are present under the primary vortex and near the symmetry plane.

The last two figures present plots of stagnation pressure and Mach number for the laminar and turbulent cases at $\alpha = 10$ deg ($X/D = 7$, Fig. 14) and $\alpha = 20$ deg ($X/D = 5$, Fig. 15). At 10 deg angle of attack, differences affect the structure of the primary vortex. If the external size of both vortices is comparable, the laminar case shows steeper gradients (Figs. 14a and 14c for stagnation pressure and Figs. 14b and 14d for Mach numbers). Values observed in the vortex core are almost identical in both cases.

At $\alpha = 20$ deg, the structure of the flow is more complex. As primary separation occurs approximately at the same location, the separated regions are very similar for the laminar and the turbulent cases. Dissipation seems to be somewhat higher in the turbulent vortex core, as the stagnation pressure is lower.

VI. Conclusion

A detailed experimental description of the flow around a missile body at incidence in a supersonic upstream flow has been made with the aim of establishing a sound physical understanding of the flow and of constituting an experimental data base. This data base will be used to validate the numerical computations based on the solution of Euler and/or Navier-Stokes equations. To permit thorough validations, the data base includes external flowfield measurements, surface pressure distributions, and characterization of the skin-friction pattern.

Experiments for a freestream Mach number of 2 have been executed both for a laminar and a turbulent boundary layer. At low-to-moderate incidences (up to 10 deg), the flow structure includes a primary vortex and a secondary vortex. At higher incidences (between 10 and 20 deg), these two vortices remain present but a more complex substructure is observed.

The greatest differences between the laminar boundary-layer flow and the turbulent flow exist at $\alpha = 5$ deg (then the turbulent flow is fully attached whereas the laminar flow separates) and at $\alpha = 10$ deg. In the turbulent case, at $\alpha = 10$ deg, the primary separation line is farther in the leeward direction, as turbulence tends to stabilize the boundary layer. The vortex structure also presents smoother gradients. This last feature induces noticeable differences on the surface pressure distribution. At higher angles of attack ($\alpha = 15$ and 20 deg), results are very similar in both cases.

Acknowledgments

This study has been performed with the financial support of the Direction des Recherches et Etudes Technique of the French Ministry of Defense. The authors are greatly indebted to the S5Ch Wind Tunnel Group for performing the experiments.

References

[1]Guillen, P., and Lordon, J., "Numerical Simulation of Separated Supersonic Flows Around Tactical Missile Bodies," AGARD Paper 88-CP-437, May 1988.

[2]Lordon, J., Faré, J.-C., and Pagan, D., "Supersonic Vortex Flows Around a Missile Body: Basic Experiment and Euler Numerical Computation," AGARD Paper 15-CP-493, April 1990.

[3]Priolo, F. J., and Wardlaw, A. B., "Supersonic Tactical Missile Computations Using Euler's Equations with Crossflow Separation Modeling," AGARD Paper 6-CP-493, April 1990.

[4]Schiff, L. B., Cummings, R. M., Sorenson, R. L., and Rizk, Y. M., "Numerical Simulation of High Incidence Flow over the F-18 Fuselage Forebody," AIAA Paper 89-0339, Jan. 1989.

[5]Deese, J., Agarwal, R., and Gielda, T., "Computation of Supersonic Viscous Flow About Missiles and Bodies at High Angles of Attack Using PNS and Navier-Stokes Solvers," AIAA Paper 89-0527, Jan. 1989.

[6]Jorgensen, L. H., and Perkins, E. W., "Investigation of Some Wake Vortex Characteristics of Inclined Ogive-Cylinder Body at Mach Number 1.98," NACA R.M. A55E31, Aug. 1955.

[7]Fidler, J. E., Schwind, R. G., and Nielsen, J. N., "Investigation of Slender-Body Vortices," *AIAA Journal,* Vol. 15, No. 12, 1977, pp. 1736–1741.

[8]Yanta, W. J., and Wardlaw, A. B., "Flowfield About and Forces on Slender Bodies at High Angles of Attack," *AIAA Journal,* Vol. 19, No. 3, 1981, pp. 296–306.

[9]Ponton, A. J. C., and Johnson, G. A., "The Analysis and Modelling of Body Vortex Flowfields Around Missile Configurations and Their Interpretation with Lifting Surfaces at Subsonic and Supersonic Speeds," Royal Aeronautical Society, Paper 26, London, 1989.

[10]Champigny, P., and Baudin, D., "Ecoulement Tourbillonnaire sur Fuselage de Missile, Etude Expérimentale et Modélisation," AGARD Paper 17-CP-494, Oct. 1990.

[11]Gaillard, R., "Etalonnage et Utilisation de Sondes Cinq Trous," *Proceedings of the 7th Symposium on Measuring Techniques for Transonic and Supersonic Flow in Cascades and Turbomachines,* Paper 16, 1983, pp. 1–17.

[12]Legendre, R., "Séparation de l'Écoulement Laminaire Tridimensionnel," *La Recherche Aéronautique,* No. 54, Nov.–Dec. 1956, pp. 3–8.

[13]Peake, D. J., and Tobak, M., "Three Dimensional Interactions and Vortical Flows with Emphasis on High Speed," AGARDograph No. 252, March 1980.

[14]Délery, J., "Physique des Écoulements Tourbillonnaires," AGARD Paper 20-CP-494, Oct. 1990.

[15]Pagan, D., and Molton, P., "Etude Expérimentale du Système Tourbillonnaire Engendré par un Fuselage de Missile en Incidence; Première Partie: Couche Limite Laminaire," Office National d'Etudes et de Recherches Aérospatiales, RT 40/1147 AY, Châtillon, France, Jan. 1990.

[16]Pagan, D., and Molton, P., "Etude Expérimentale du Système Tourbillonnaire Engendré par un Fuselage de Missile en Incidence; Deuxième Partie: Couche Limite Turbulente," Office National d'Etudes et Recherches Aérospatiales, RT 42/1147 AY, Châtillon, France, June 1990.

Gerald T. Chrusciel
Associate Editor